Simulating the Effects of Irrigation over the United States in a Land Surface Model Based on Satellite-Derived Agricultural Data

MUTLU OZDOGAN

Center for Sustainability and the Global Environment (SAGE), University of Wisconsin—Madison, Madison, Wisconsin

MATTHEW RODELL

Hydrological Sciences Branch, NASA Goddard Space Flight Center, Greenbelt, Maryland

HIROKO KATO BEAUDOING

Hydrological Sciences Branch, NASA Goddard Space Flight Center, Greenbelt, and Earth System Science Interdisciplinary Center, University of Maryland, College Park, College Park, Maryland

DAVID L. TOLL

Hydrological Sciences Branch, NASA Goddard Space Flight Center, Greenbelt, Maryland

(Manuscript received 20 October 2008, in final form 8 August 2009)

ABSTRACT

A novel method is introduced for integrating satellite-derived irrigation data and high-resolution crop-type information into a land surface model (LSM). The objective is to improve the simulation of land surface states and fluxes through better representation of agricultural land use. Ultimately, this scheme could enable numerical weather prediction (NWP) models to capture land–atmosphere feedbacks in managed lands more accurately and thus improve forecast skill. Here, it is shown that the application of the new irrigation scheme over the continental United States significantly influences the surface water and energy balances by modulating the partitioning of water between the surface and the atmosphere. In this experiment, irrigation caused a 12% increase in evapotranspiration (QLE) and an equivalent reduction in the sensible heat flux (QH) averaged over all irrigated areas in the continental United States during the 2003 growing season. Local effects were more extreme: irrigation shifted more than 100 W m^{-2} from QH to QLE in many locations in California, eastern Idaho, southern Washington, and southern Colorado during peak crop growth. In these cases, the changes in ground heat flux (QG), net radiation (RNET), evapotranspiration (ET), runoff (R), and soil moisture (SM) were more than 3 W m^{-2}, 20 W m^{-2}, 5 mm day^{-1}, 0.3 mm day^{-1}, and 100 mm, respectively. These results are highly relevant to continental-to-global-scale water and energy cycle studies that, to date, have struggled to quantify the effects of agricultural management practices such as irrigation. On the basis of the results presented here, it is expected that better representation of managed lands will lead to improved weather and climate forecasting skill when the new irrigation scheme is incorporated into NWP models such as NOAA's Global Forecast System (GFS).

1. Introduction

Land surface conditions govern moisture, heat, and momentum exchanges between the surface and atmosphere greatly influencing global weather patterns that further affect our society. By modulating surface–atmosphere exchanges of heat and water, agricultural land management can significantly influence the climate system and the hydrological cycle (Bonan 1997, 2001; Chase et al. 2000). In particular, cropland irrigation has been shown to affect local and regional climates and hydrology by modifying the partitioning of water between the surface and the atmosphere (Pielke and Zeng 1989; Otterman et al. 1990; Ben-Gai et al. 2001; Moore and Rojstaczer 2002; Ozdogan et al. 2006; Lobell and

Corresponding author address: Mutlu Ozdogan, SAGE, University of Wisconsin—Madison, 1710 University Avenue, Madison, WI 53706.
E-mail: ozdogan@wisc.edu

DOI: 10.1175/2009JHM1116.1

Bonfils 2008; Kueppers et al. 2008; Lobell et al. 2008). At larger scales, however, the climatic and hydrologic effects of irrigated croplands are still poorly understood.

Numerical weather prediction (NWP) and climate models have adopted progressively more sophisticated representations of land surface processes over the course of past the two decades (e.g., Dickinson and Henderson-Sellers 1988; Sellers et al. 1996; Bonan et al. 2003; Ek et al. 2003). These land surface models (LSMs) simulate the behavior of complex and highly variable (in both space and time) surface states—such as soil moisture (SM), temperature, and snow water—and provide initial and updated conditions to simulations of large-scale atmospheric processes. However, despite progressive improvement of input variables, treatment of vegetation, and soil physics, today's LSMs largely ignore the effects of irrigation and other land management practices on an operational basis. Herein we describe an original technique for applying satellite-derived irrigation data and high-resolution crop-type information within a LSM, and we evaluate its effects on modeled land surface states and fluxes. With the research presented here, our objective is twofold: to assess the effects of irrigation and land management on LSM-derived states and fluxes, and to improve the representation of managed lands in land surface schemes.

2. Background

A number of studies used numerical model simulations to study the effects of irrigation within both uncoupled and coupled (from the atmosphere) experiments. The majority of uncoupled experiments concentrated on irrigation's influence on hydrological fluxes and states. For example, Mahmood and Hubbard (2002) investigated the effects of irrigated agriculture on near-surface hydrological cycle components using a simple soil moisture model. They found that irrigated croplands impart much more water to the atmosphere via evapotranspiration than natural grasslands in unaltered landscapes. In another uncoupled study, de Rosnay et al. (2003) showed that intensive irrigation has a regional impact on the partitioning of energy between sensible and latent heat fluxes, and they pointed out that irrigation can be a major factor in the water cycle. Their model was developed to take into account the interactions between water demand and land and atmospheric processes, which together define water availability. Haddeland et al. (2006) developed an irrigation scheme for the Variable Infiltration Capacity (VIC) LSM based on simulated soil moisture deficit. Application of the scheme to the Colorado and Mekong River basins showed that, in general, irrigation leads to decreased streamflow and increased evapotranspiration. They also demonstrated that although increases in basin-averaged latent heat flux were small, irrigation caused locally significant increases (up to 60%) in evapotranspiration that reduced surface temperatures, and hence decreased sensible heat flux. More recently, Tang et al. (2007) investigated the effects of natural and anthropogenic heterogeneity (including irrigation) on a hydrological simulation using a distributed biosphere hydrological model system. The results suggest that irrigation leads to increased evapotranspiration, decreased runoff, increased surface soil moisture, and decreased streamflow. In concert with previous studies, the average latent heat flux in the peak irrigation season increased only slightly; however, the maximum simulated increase in the latent heat flux exceeded 40 W m^{-2} with a strong consequence of ground temperature decrease.

Irrigation has also been studied in coupled modeling experiments. Early coupled experiments simply kept a portion of land surface wet under idealized conditions (Yeh et al. 1984). Recent experiments have been more sophisticated. For example, Segal et al. (1998) used a top–down approach to irrigation, imposing a fixed amount of evapotranspiration from irrigated lands under ideal conditions during the growing season to assess feedbacks to summer precipitation. Results indicated that the effects of irrigation on rainfall are mostly nonlocal, and that irrigation is more likely to augment existing weather systems than trigger new ones. In an irrigation impact study using the Colorado State University Regional Atmospheric Modeling System (RAMS), Adegoke et al. (2003) found significant differences in the regional average surface energy fluxes between the control (irrigated) and the dry (nonirrigated) experiments in central Nebraska. Monthly mean and daily maximum temperatures for the irrigated site steadily decreased during the growing season in contrast to an increasing trend at the nonirrigated site. Chen and Avissar (1994) investigated the formation of mesoscale circulations induced by landscape discontinuities, specifically in the form of dry and wet patches that are present in irrigated areas, and they concluded that these circulations are strongly related to the variability of mesoscale heat fluxes into the planetary boundary layer. Thus, to capture cloud development, radiation balance, and other boundary layer processes in atmospheric models, their study suggested that the locations and patterns of landscape heterogeneities—patterns of irrigation in particular—should be represented in coupled models. More recently, Kueppers et al. (2007) used a regional climate model to show that irrigation can have a cooling effect in the dry season and concluded that in California, ''past expansion of irrigated land has likely affected observations of surface temperature, potentially masking the full warming signal caused by

greenhouse gas increases.'' Kueppers et al. (2008) also reported on the seasonally varying temperature responses of four regional climate models to irrigated agriculture development in the western United States. Overall, irrigation produced large decreases in air temperature and large increases in relative humidity in midsummer months, but different models had varying responses to irrigation. Similarly, Kanamaru and Kanamitsu (2008) examined the mechanisms of nighttime minimum temperature warming in California during summer due to irrigation and concluded that ground heat flux efficiently keeps the surface warm during nighttime because of increased thermal conductivity of wet soil. Lastly, Weare and Du (2008) explored the influences of global warming and land use changes on past climate change in California and conclude that in summer, irrigation has a strong effect on the differences between recent and past conditions in maximum temperature, surface latent and sensible heat fluxes, surface moisture, and surface humidity.

As evident in their nature, previous studies on irrigation within numerical models tend to fall into two categories: uncoupled, small scale, and more realistically parameterized experiments at local scales (e.g., Haddeland et al. 2006); and coupled, larger-scale experiments with highly simplified representations of irrigation (e.g., Lobell et al. 2006). The advantages of the latter are ease of implementation and computational efficiency, at the expense of realism. Here, we introduce a realistic yet portable irrigation scheme and demonstrate its efficacy in a land surface model (Noah) that is used operationally for (coupled) weather prediction. A major advantage of the new scheme is its implementation at a nearly continental scale based on an accurate satellite-derived map of irrigation intensity, as well as its operation status within numerical weather prediction models.

3. Data

a. Satellite-derived irrigation intensity

The primary objective of this study is to quantify the effects of irrigation on land surface states (e.g., soil moisture and temperature) and fluxes (e.g., evapotranspiration and runoff) by implementing a realistic irrigation scheme within an uncoupled land surface model. The first requirement to achieve this objective is an accurate, objective, contemporary map of irrigation intensity and extent. Most existing irrigation maps were compiled from county-level statistics that are often outdated (Siebert et al. 2007), or they were produced using coarse-resolution satellite data (Thenkabail et al. 2008). Even in regions, such as the United States, where irrigation statistics are generally reliable and well documented, the disparate information cannot be easily synthesized into a single continental-scale database. To overcome these limitations, this research uses a new high-spatial-resolution irrigation dataset derived from satellite observations. The details of the new dataset are provided by Ozdogan and Gutman (2008). In short, the dataset was generated by merging gridded climate datasets and remotely sensed observations from the Moderate Resolution Imaging Spectroradiometer (MODIS) instrument on board the National Aeronautics and Space Administration (NASA)'s *Terra* satellite within an image classification algorithm. The new dataset is objective, accurate, and characterizes the distribution of per-pixel fractional area of irrigated lands in the continental United States *circa* 2001 at relatively high (500 m) spatial resolution.

b. Land cover

The land cover classification dataset used in the experiments was generated by merging gridded land cover and crop-type distribution databases. The land cover database is a static, 1-km resolution global map of land cover classes produced at the University of Maryland (UMD) based on observations from the Advanced Very High Resolution Radiometer (AVHRR) on board the National Oceanic and Atmospheric Administration (NOAA)'s satellite *NOAA-15* (Hansen et al. 2000). The UMD classification scheme includes 11 vegetation classes, bare ground and urban land cover classes, and water. Although the UMD land cover map includes a ''cropland'' land cover class, it does not distinguish different crop types—let alone the irrigation status of those crop types. In reality, each type of crop has distinct irrigation water requirements and timing that vary with the climate. Using an average crop type in an irrigation simulation scheme could cause grossly over- or underestimated water input. To remedy this issue, we developed a new global dataset that categorizes crop-type distributions within the UMD land cover map. The basis for crop categorization was a crop-type database (hereafter CROPMAP) that consists of 5-min (~10 km) resolution maps of the distributions of 19 different crops in which each crop-type layer describes that crop's intensity at each pixel as a percentage of all crops (Leff et al. 2004). CROPMAP is a synthesis of crop-specific agricultural census data and spatially explicit data on the extent of the world's croplands. It represents a first-order global database that is generally consistent with common agricultural knowledge and is also largely consistent with U.S. Department of Agriculture (USDA) reports.

To generate a gridded land cover map that includes information on specific crop types, we merged the UMD map with the CROPMAP as follows. For every 5-min

CROPMAP grid, we applied the appropriate percentage distribution of the 19 crops to the roughly one hundred 1-km UMD cropland pixels randomly space. For example, within a CROPMAP cell that contained 60% maize and 40% soy, we randomly assigned 60 of the corresponding UMD cropland pixels to maize and 40 to soy. In cases of inconsistency between the two datasets, the UMD classification took precedence. That is, when the UMD dataset had no crop pixels in a given 5-min cell, no crops types were imposed, regardless of the CROPMAP information. When the UMD map indicated that crops existed but CROPMAP did not, UMD cropland pixels were prescribed as wheat, reasoning that wheat is the most widespread crop type in the United States. Inconsistencies between the two datasets were infrequent and thus not a significant source of error. To quantify the rate of inconsistency, the newly generated 1-km land cover map was aggregated to 5-min spatial resolution, and in all cases, the percentage of crop types was within 5% of that reported in the original CROPMAP dataset.

The new land cover database is a single-layer dataset with ~1-km spatial resolution, representing 31 land cover classes (12 UMD land cover classes + 19 crops). To meet the input requirements of the Land Information System (LIS) model driver (described in detail in section 4a), the merged 1-km dataset was aggregated to a 0.125° model grid by counting the number of pixels of each land cover class in each 0.125° grid square.

c. Meteorological forcing

The North American Land Data Assimilation System (NLDAS) forcing dataset (Cosgrove et al. 2003) was used to drive the simulations. The dataset covers the continental United States and parts of Canada and Mexico (25°–53°N, 125°–67°W) at 0.125° and hourly resolutions. It consists of numerical weather prediction model outputs and observation-based products that are blended and interpolated to the required resolutions. The baseline forcing fields are generated by the National Centers for Environmental Prediction (NCEP) Eta Data Assimilation System (EDAS; Rogers et al. 1996) or the Eta Model when EDAS is not available. The precipitation and radiation fields are replaced by observation-based data as available. The NOAA Climate Prediction Center (CPC) daily gauge data (Higgins et al. 2000) are downscaled to hourly resolution using stage II Doppler radar data (Baldwin and Mitchell 1997). The downward shortwave radiation data are derived from Geostationary Operational Environmental Satellite (GOES) observations (Pinker et al. 2003). An elevation adjustment is applied to the surface pressure, longwave radiation, 2-m temperature, and humidity fields to account for discrepancies in topography between EDAS/Eta and NLDAS due to their differing spatial resolutions.

4. Methods

a. Land surface model and driver

Experiments were performed with the Noah LSM (version 2.7) running within the LIS. LIS is a highly efficient and parallelized model driver that allows users to run multiple LSMs locally and globally, at various resolutions (from 1 km to 2.5°), using a variety of forcing options from a common software interface (Kumar et al. 2006). LIS has its roots in the NLDAS [Mitchell et al. 2004 and the global LDAS (GLDAS); Rodell et al. 2004], which have since adopted the LIS software. LIS divides grid pixels into ''tiles'' based on land cover to simulate subgrid-scale heterogeneity, hence the requirement for a high-resolution land cover (and crop) database. LIS/Noah proceeds as a series of single-column simulations on the subgrid tiles with no horizontal interactions. Soil texture is based on the United Nations' Food and Agriculture Organization (FAO) soil database (Reynolds et al. 2000). Elevation parameters are derived from a global 30-arc-second resolution topographic map (Gesch et al. 1999). LIS is fully modularized and compliant with Earth System Modeling Framework (ESMF) and Assistance for Land Surface Modeling Activities (ALMA) standards, making it an ideal platform for developing innovative modeling and assimilation capabilities, including simulated irrigation.

The Noah LSM (Chen et al. 1996; Koren et al. 1999) was developed beginning in 1993 through a collaboration of investigators from public and private institutions, spearheaded by NOAA's NCEP. Noah is a stand-alone, 1D column model that can be executed in either coupled or uncoupled mode. The model applies finite-difference spatial discretization methods and a Crank–Nicholson time-integration scheme to the equations that describe the physical processes of the soil, vegetation, and snowpack. Outputs are the stocks and fluxes of the near-surface water and energy budgets. Noah has been used operationally in NCEP models since 1996, and it continues to benefit from a steady progression of improvements (Betts et al. 1997; Ek et al. 2003).

b. Simulating irrigation

The three key aspects of irrigation in a modeling framework are the irrigation trigger (when to irrigate), amount (how much to irrigate), and the method (e.g., rain, spray, drip; and rate). In the United States and much of the modernized world, farmers often use 30–40-cm soil moisture sensors to assess plant available moisture in the

upper-root zone and to irrigate when soil moisture falls below a prescribed threshold. Farmers without moisture sensors either use traditional indicators of soil dryness (e.g., soil color, wilting) or irrigate on a set schedule during periods lacking sufficient rainfall.

Following actual irrigation practices in the United States, irrigation in our scheme is triggered when the root-zone soil moisture falls below a threshold, in essence replicating a moisture sensor scenario. The root-zone moisture availability (MA) is defined as ratio of the difference between the current root-zone SM and the wilting point (SM_{WP}) and the difference between field capacity (SM_{FC}) and SM_{WP}:

$$MA = (SM - SM_{WP})/(SM_{FC} - SM_{WP}). \quad (1)$$

Field capacity (the maximum amount of water that the unsaturated zone of a soil can hold against the pull of gravity) is a parameter that Noah prescribes based on soil type. We chose 50% of field capacity as the irrigation trigger threshold based on discussions with local experts in Nebraska and California, followed by trial and error (not shown). The depth of the root zone varies in time according to the plant's growth cycle. Maximum root-depth values were assigned based on published coefficients, replacing Noah's default values, and they are used in the calculations of ''current'' soil moisture availability. By scaling the maximum root depth with the greenness fraction, the seasonal variability in the root zone is captured. This is necessary because growing season consumption and utilization of water by a crop is largely determined by the expansion of leaf area (represented by greenness fraction) and root depth during phenological development. Hence, phenological development influences transpiration rates, the soil wetness profile, and the water and energy balances.

The irrigation scheme begins by checking if the current tile represents cropland or another potentially irrigated land class (e.g., grass), and whether or not the encompassing grid cell is irrigated. The scheme then determines if it is the growing season. The growing season begins and ends when a threshold of 40% of annual range of greenness fraction at the grid cell is crossed. Most agricultural areas in the United States have growing seasons between April and October; however, some locations in the southwestern United States have elongated growing seasons that begin earlier. Next, if MA is below the irrigation trigger, the scheme computes the irrigation requirement for each subgrid tile as an equivalent height of water by subtracting the current root-zone soil moisture from the field capacity. If the ratio of irrigated area to total crop coverage in the encompassing grid cell is less than one, then the irrigation requirement for each tile is reduced by the same ratio. Conversely, if that ratio is greater than one, then the tile-area-weighted gridcell total irrigation requirement is scaled up by the ratio, and the additional water is first applied to grassland, if such a tile exists. Any remaining water (beyond the field capacity of the grassland tile) is applied evenly to other noncrop tiles, excluding forests, bare soil, and urban tiles. This approach was chosen primarily to account for the misclassification of agricultural areas, based on our assumption that the irrigation map is more reliable than the land cover map. We surmised that distinguishing grassland from cropland using satellite imagery would be especially prone to error. Further, in the cases of golf courses, sod farms, and perhaps other land uses, grass and irrigation are not mutually exclusive. To illustrate the approach, given a grid cell with 60% irrigation intensity and wheat, soy, grassland, and forest tiles covering 30%, 20%, 40%, and 10% of its area, each at 10 mm below field capacity, the scheme would apply 10-mm irrigation to the wheat and soy tiles and [10 mm * (60% − 30% − 20%)/40%] = 2.5 mm to the grassland tile. In this example, a uniform 10 mm requirement is used for the sake of simplicity. In actuality, root-zone depth varies by land cover type and greenness fraction, so crop tiles are likely to have different irrigation requirements.

The irrigation trigger is evaluated daily at 0600 local time. If positive, the irrigation requirement is applied as precipitation (i.e., sprayed from above) at a uniform rate between 0600 and 1000 LT., a time frame typically chosen by farmers to reduce evaporative losses. Other than the efficiency, the resulting states and fluxes are not likely to differ much from an algorithm that applies the irrigation directly to the soil, because we allow some water to evaporate and runoff before it starts percolating through soils, as that would happen in spray irrigation. A preliminary test (not shown) of applying water directly to soil moisture resulted in too much irrigation water for the Midwest, which may be partially explained by pressure (spray) irrigation being the most common method of water delivery in the country. The irrigation scheme is invoked at each (15 min) time step before the LSM is called. We assumed that water resources are freely available for irrigation (i.e., from surface or ground waters—reservoirs that are not simulated in Noah 2.7.1). Further, the amount applied is effectively the net irrigation—that is, after on-the-field and transportation losses.

c. *Experimental design*

Three experiments were performed to assess the effect of agricultural land management on hydrological

fluxes: *control*, *crops*, and *irrigation*. Both the crops and irrigation experiments used the new UMD-CROPMAP dataset, whereas control used the original UMD dataset with a single ''average'' crop class. No irrigation was applied in the control and crops experiments. The CROPMAP was required for the scheme to determine how much irrigation to apply to a given irrigated area. The purpose of the control experiment was to isolate the effect of adding a realistic array of crop types. That effect turned out to be minor—that is, the control and crops experiments produced similar results—hence, the control experiment will not be discussed in detail in the remainder of this paper. The effect of irrigation is demonstrated through comparisons between the crops and irrigation experiments. The effective domain was the continental United States, gridded at 0.125° resolution, and the experimental period was 2003. The 1-km UMD and UMD-CROPMAP datasets were used to define subgrid tiles. In all experiments, a minimum grid coverage threshold of 5% was assigned in determining the number and types of tiles; that is, vegetation classes that covered less than 5% of a given grid cell were not modeled. The vegetation parameter file in Noah was augmented with the new values for the 19 crop types. Some of these parameters (e.g., root depth and roughness length) are physical and were acquired from the literature, whereas others are nonphysical and specific to the Noah model, making them difficult to estimate. For example, in the control experiment, root depth for the average crop class extends to layer 3 and roughness length is 0.035 m. In the crops and irrigation experiments with explicit crop types, some crops have root depth extending beyond the third soil layer and roughness lengths are higher than 0.035 m, as in the average crop. However, for some of the latter type, we used Noah's value for cropland land cover as the default. The model time step was 15 min, and output was recorded hourly. The model was spun up from 1996 to 2002 using the NLDAS forcing data.

In addition to the three national-scale experiments, two sets of single gridcell (point) simulations using the same crops and irrigation schemes were performed for comparison with field data. These data were collected at an irrigated maize site in Mead, Nebraska (41.17°N, 96.48°W), which is part of the AmeriFlux observational network, and at an irrigated grassland site in Five Points, California (36.34°N, 120.11°W), which is maintained by the USDA. Each point simulation was forced by NLDAS data, with the same spin-up procedure previously described. They differed from the national scale simulations in that they included only a single tile whose land cover type matched that at the field site, and the Five Points simulation continued through 2004 and 2005, the two years for which data were available for that site.

5. Results

a. Irrigation water requirements

Accurately representing the amount, location, and timing of water applied is essential for simulating irrigation and quantifying its effect on hydrological fluxes and state variables. Comparison of our predicted irrigation requirements with those compiled for the United States at the county level (Hutson et al. 2004) demonstrates that there is generally good agreement between reported irrigation and that applied by our scheme, both in terms of spatial extent (Fig. 1) and amount (Fig. 2). The root-mean-square error (RMSE) is less than 0.3 $km^3\ yr^{-1}$ per county, which is reasonable given that the satellite data do not directly indicate the volume of water irrigated. Further, the scheme exhibits low bias (0.012 $km^3\ yr^{-1}$), which gives us confidence in its ability to simulate real-world irrigation—both in terms of location and amount. Note that our simulation year (2003) and the reported estimates from the Hutson et al. (2004) are not from the same year. Given interannual climate variations, it is likely that these two datasets do not represent the same irrigation amount values. However, comparison of the USGS values to the USDA 2003 Farm and Ranch Irrigation Survey (USDA 2004; not shown) at the state level yields comparable estimates of irrigation water and thus lends credibility to our comparisons.

Averaged over the entire country, irrigation peaks in July and August, driven by strong summer insolation, high temperatures, and maturing crops in three different regions (Fig. 3). This seasonal cycle predicted by the irrigation scheme is intuitive and is corroborated by reported irrigation totals (USDA 2004). Irrigation requirements are a function of crop types and climate, which vary across regions. Model-predicted volume of irrigation water is largest in the central region (110°–95°W) and slightly less in the western region (124°–110°W), and this volume is the smallest in the east (95°–67°W). This is in contrast to the reported irrigation quantities from the USDA (2004), shown as gray horizontal bars on Fig. 3, which suggests higher irrigation volumes in the western region than in the central region. We explain this inconsistency between reported and estimated irrigation volumes by the coarse nature of the greenness fraction data, which affects the timing of irrigation as well as the lack of model's ability to capture high-water-demand agriculture, such as vegetables in the western region (mainly in the state of California). Nevertheless, this under- and overestimation of irrigation

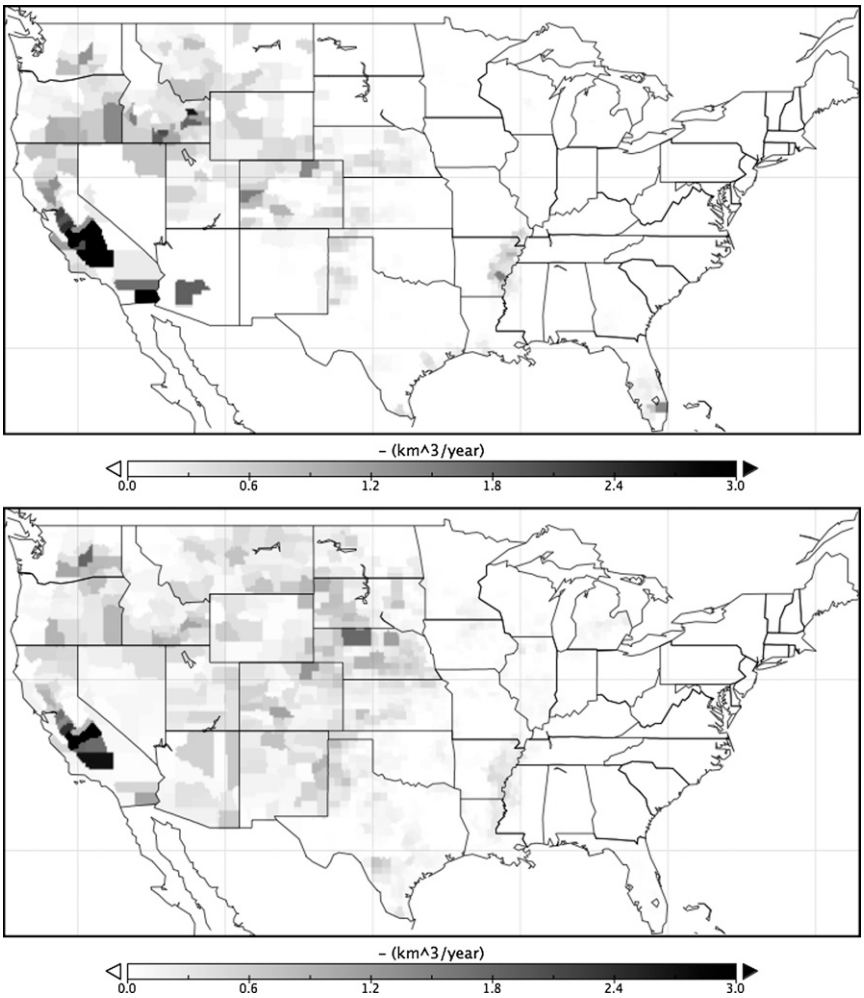

FIG. 1. Geographic patterns of annual irrigation water use ca. 2000 (top) reported by the USGS and (bottom) modeled in this study at the county level in cubic kilometers.

volumes does not minimize the main statement of our findings, which suggest that irrigation greatly influences the water and energy budgets of the land surface that are so important for land–atmosphere interactions and local climate.

With respect to the timing of irrigation, in the western United States, irrigation demand shows relatively little high-frequency variability, increasing quickly from May through early July and then gradually decreasing through October. The most heavily irrigated area in the west is California's Central Valley, which is dominated by vegetables and orchards with extended growing seasons. The dominant crop in the northern part of the western region is wheat. Western agriculture's constant dependence on irrigation, particularly in California, owing to a dry season that extends from May to October, accounts for the relative smoothness of the plot of irrigation rates. Its early peak corresponds with an early peak in greenness fraction, which occurs near the end of June. In the central region, the irrigation rate increases in spring, followed by a larger increase throughout summer, and a sharp decline in the fall. Here, the dominant crop types are maize and soybeans, which exhibit a strong summer demand for irrigation. In contrast, the eastern region typically has much lower irrigation demand because of its more humid climate.

b. Irrigation effects on energy and water budget components

Irrigation raises the soil water content, enabling evapotranspiration, which in turn transforms the energy budget. Simulated increases in evapotranspiration due to the new irrigation scheme are presented in Fig. 4 as a series of monthly maps. The temporal and geographical features described in the previous section are evident. In general, peak increases in evapotranspiration occurred

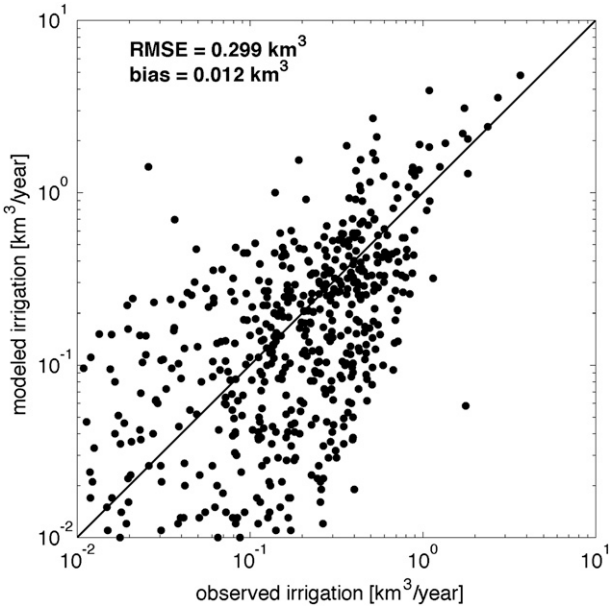

FIG. 2. Comparison of irrigation scheme–predicted annual water use to the reported values at the county level. The reported data are from the USGS. Note that the data are presented in log scale to show both small and large water use estimates that occur across counties. Each dot represents a county's annual water use in cubic kilometers. RMSE and bias of the model results are also shown.

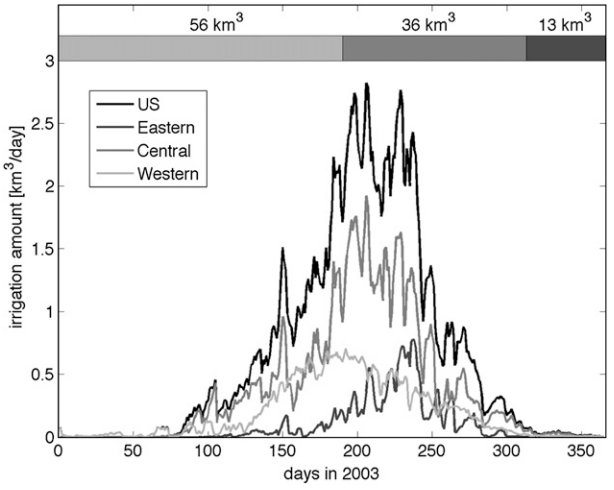

FIG. 3. Modeled daily total irrigation amounts (km^3 day^{-1}) accumulated over the United States (black) and three regions: eastern (95°–67°W); central (110°–95°W), and western (124°–110°W). Also shown is the volume of USDA-reported annual irrigation amounts in these three regions for the same year. The bar shades match the shades of time plots.

in July and August, though the region of heavy irrigation in the southeastern United States along the Mississippi River lagged in phase. In parts of California, Washington, Indiana, Colorado, Nebraska, South Dakota, and North Dakota, evapotranspiration increased by at least 100% of the crops simulation during the summer peak. In one extreme case, evapotranspiration in a pixel in California jumped from 1.44 to 177 mm $month^{-1}$.

The majority of current LSMs do not include explicit crop types, thus their ''crop'' vegetation parameters are meant to be representative of the average. However, explicit description of crop types appears to affect simulation of both water and energy budgets (not shown). Increasing the number of crop types to 19 and specifying new parameters for each generally shifted energy or water balance components in the same direction as simulating irrigation—but to a much lesser amount. However, the mean SM values in the control and irrigation experiments were nearly equivalent, whereas the crops experiment means were consistently lower. This highlights the importance of realistically simulating crops, which, in the case of the Noah model, enables more root uptake and transpiration, and hence results in a drier root zone (in the absence of irrigation).

Averaged over all irrigated areas in the continental United States and over the growing season (April–October), irrigation increased latent heat flux (QLE) by 9 W m^{-2} (or 12% of QLE from crops experiment), decreased sensible heat flux (QH) by 8 W m^{-2} (11%), and slightly increased ground heat flux (QG) by 0.05 W m^{-2} (2%) and net radiation (RNET) by 1.2 W m^{-2} (0.8%). To balance the extra input of water, evapotranspiration (ET) rose by 0.3 mm day^{-1} (or 12% of crops experiment), runoff (R) by 0.01 mm day^{-1} (5%), and total column SM by 15 mm (4%). As with irrigation itself, these effects were most pronounced in July and August. At their peak in August, QLE and ET increased by 26%, QG by 5%, RNET by 2%, R by 11%, and SM by 7%, and QH decreased by 18%.

Diagnostics are included in Fig. 5 for the same three regions previously defined: western, central, and eastern United States. Because the western agricultural regions are relatively arid, on average, they received the most irrigation per unit irrigated area, and accordingly, the effects were greatest. Both irrigation rate and effects were most pronounced in the Central Valley of California, which skewed the western averages. Save for SM, the effects of increasing crop types were greatest in the eastern region. Local effects were sometimes extreme. For example, irrigation shifted more than 100 W m^{-2} from QH to QLE in the energy balance of many locations in California in July. In these cases, the changes in QG, RNET, ET, R, and SM were more than 3 W m^{-2}, 20 W m^{-2}, 5 mm day^{-1}, 0.3 mm day^{-1}, and 100 mm, respectively. Effects of similar magnitude were also seen in eastern Idaho, southern Washington, and southern Colorado.

We also compared the ability and outcome of the irrigation module over individual sites for which detailed

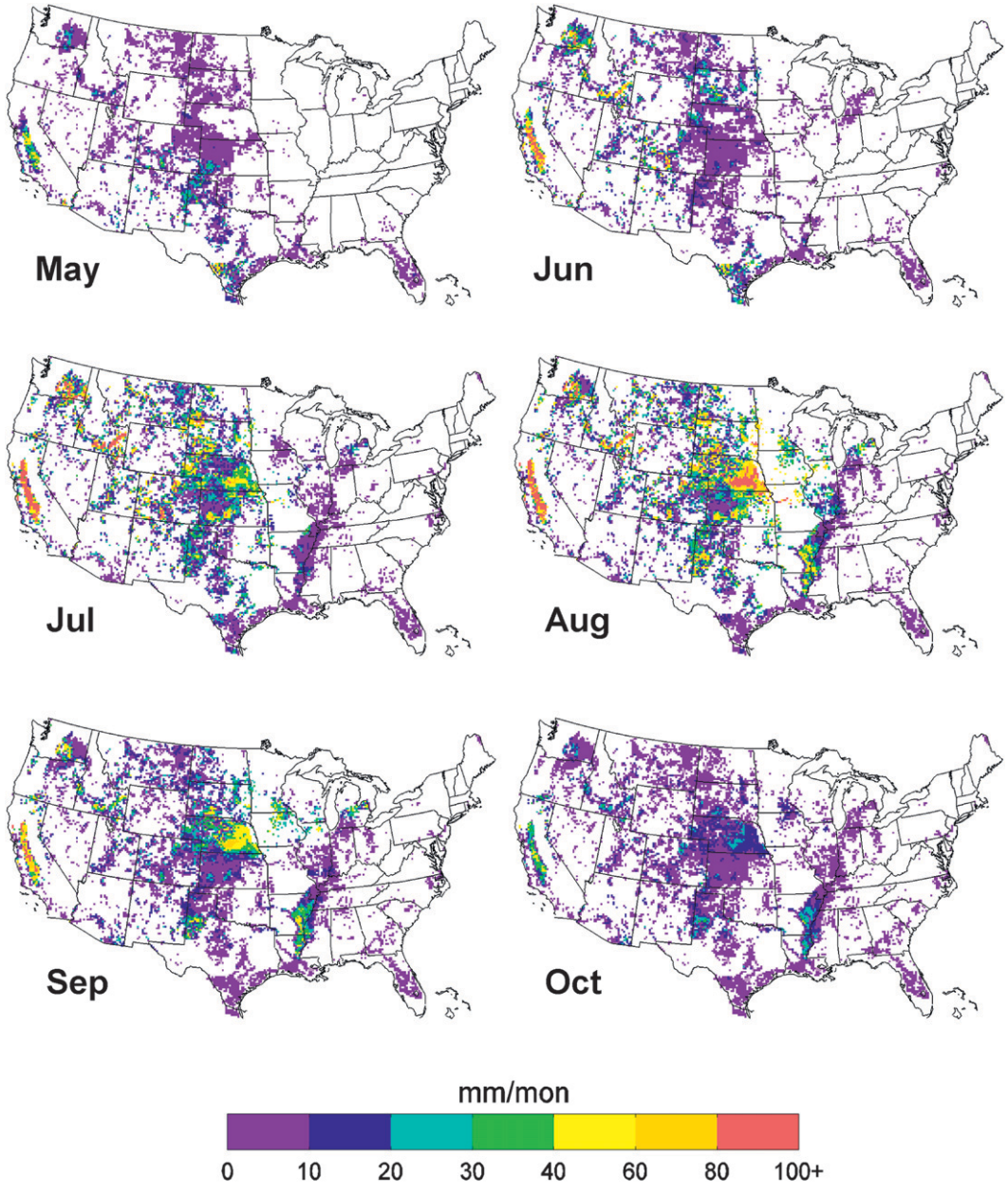

FIG. 4. Difference between simulated monthly evapotranspiration totals (mm month^{-1}) from the irrigation and crops (19 crops) experiments for May through October 2003.

information exists. One such site is an AmeriFlux site near Mead, Nebraska (Fig. 6). Here, volumetric soil moisture in the crops experiment followed a normal summertime drying trend, interrupted by rainfall events. However, observations from the site indicate that irrigation kept soil moisture near saturation. The scheme predicted irrigation on 11 days, totaling 396 mm of water between July 1 and August 31. This agrees remarkably well with the reported irrigation frequency (12 days) and total (345 mm), despite a few early mismatches between NLDAS and observed rainfall, which hampered the scheme's ability to predict the exact days when irrigation was applied. Simulating irrigation dramatically increased soil moisture, maintaining it within approximately the same range as that of observed, suggesting significant improvements in modeled soil moisture and fluxes with the irrigation scheme (Fig. 6).

Presence of irrigation also improved simulated diurnal cycles of latent and sensible heat fluxes at the Mead field site as compared to observations (Figs. 7a

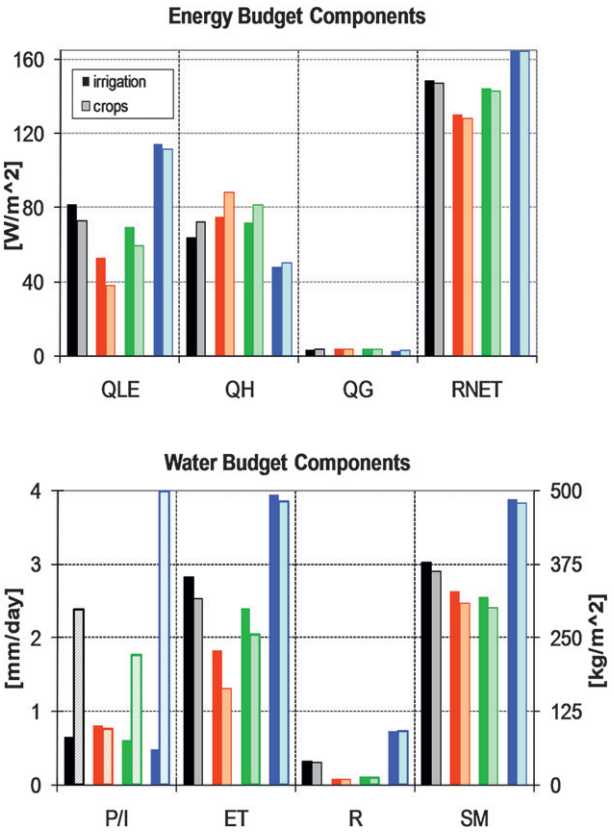

FIG. 5. Growing season (top) mean energy and (bottom) water budget components averaged over irrigated areas of the United States, from the irrigation (solid dark color) and crops (solid lighter shade) experiments. Energy budget components include QLE, QH, QG, and RNET. Water budget components include precipitation (P; slashes), irrigation (I; solid), ET, R, and total column SM. The bottom figure has y axes for (left) P/I, ET, and R and (right) SM. Regions are color coded for all irrigated area (black), eastern (95°–67°W) (blue), central (110°–95°W) (green), and western (124°–110°W) (red) U.S. irrigated area. All simulations were forced by the same precipitation dataset.

and 7b). The amplitude of the crops experiment latent heat flux at midday was underestimated by about 200 W m^{-2}, whereas the sensible heat flux was overestimated by about 340 W m^{-2}. When the irrigation scheme was engaged, those errors reduced to within 80 W m^{-2}, and the shape of the diurnal cycle of sensible heat flux greatly improved.

The effects of irrigation in California's central valley are also dramatic. At the Five Points irrigated grassland site, ET was measured using a weighing lysimeter (Vaughan et al. 2007) during 2004 and 2005. The site received no significant accumulation of rain during the summers of those years. Consequently, the crops experiment generated dry soils and near-zero ET in August of both years (Figs. 7c and 7d). When the irrigation scheme was activated, the additional moisture enabled Noah's diurnal cycle of ET to approximate the observations reasonably well, with a 15% low bias in 2004 and a 25% low bias in 2005. The irrigation scheme alleviated corresponding high biases in sensible heat flux and surface temperature (not shown).

Similar changes were also evident in the national-scale simulations. Although the crops experiment overestimated daytime land surface temperature in most irrigated regions, the irrigation experiment produced results more consistent with observations based on the following normalized temperature difference metric:

$$\mathrm{DLST}_{\mathrm{model-obs}} = |\mathrm{LST}_{\mathrm{crops}} - \mathrm{LST}_{\mathrm{GOES}}| - |\mathrm{LST}_{\mathrm{irr}} - \mathrm{LST}_{\mathrm{GOES}}|. \quad (2)$$

In (2), $\mathrm{LST}_{\mathrm{crops}}$ and $\mathrm{LST}_{\mathrm{irr}}$ refer to land surface temperature predicted by the crops (or control) and irrigated runs respectively and $\mathrm{LST}_{\mathrm{GOES}}$ is the land surface temperature observed by the GOES instrument. Accordingly, incorporating irrigation with the new scheme decreases the land surface temperature averaged over the 13-day period between 13 and 25 August 2003 at 1800 UTC, in essence reducing land surface temperature prediction errors on the order of 10 K when compared to satellite observations (depicted as positive values in Fig. 8). Note that because of inherent difficulties in modeling the land surface energy balance, there are expected differences between the two surface temperature estimates. However, these differences between GOES and modeled LST are the reason we chose to depict the improvements following Eq. (2)—these improvements are much easier to see when decoupled from all GOES model differences. Although Fig. 8 does show differences over nonirrigated areas, these areas are not relevant to the present study.

6. Discussion

The results demonstrate that irrigation significantly modulates the water and energy budgets of the land surface, in agreement with conclusions of previous studies. The primary innovation of this work is a computationally efficient yet sufficiently realistic irrigation scheme based on satellite observations of irrigation intensity, which has already been implemented over the continental United States and which will be straightforward to apply globally once the irrigation intensity map has been extended. It has been shown that by employing a simple set of rules based on actual practices to determine when and how much to irrigate, the scheme reasonably approximates reported irrigation water application rates. This provides a measure of confidence

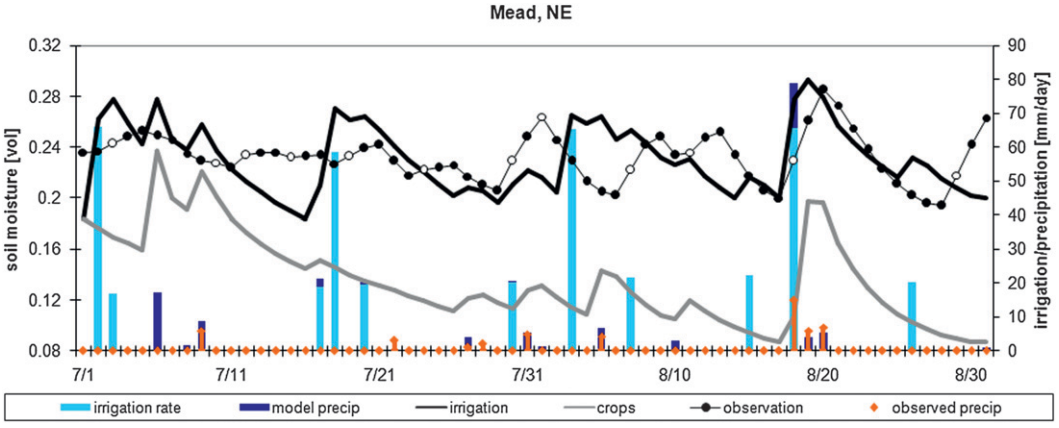

FIG. 6. Time series of (left axis) volumetric soil moisture content and daily total irrigation and precipitation (mm day^{-1}) at an irrigated (maize) AmeriFlux site in Mead, Nebraska. The irrigation (black line) and crops (gray line) soil moisture outputs are from the top layer, 0–10-cm depth, for the pixel containing the field site (55% maize, 20% soy, 19% wheat, and 6% sorghum). Soil moisture observations (black dots) were measured at 10 cm. Open black dots indicate days when irrigation was applied at the field site. The model forcing (NLDAS) precipitation (medium blue bars) is on top of the irrigation amount (light blue bars). Observed precipitation (orange dots) was taken from the automated station data at the nearby meteorological station.

that the scheme will produce useful results in parts of the world where irrigation data are not available, though it may have to be optimized for crops not grown widely in the United States, such as rice.

The Noah LSM, used here, is the land component of NOAA's Global Forecast System (GFS; NOAA 2005). It improves the skill of NOAA's short-term and seasonal forecasts by simulating the behavior of complex and

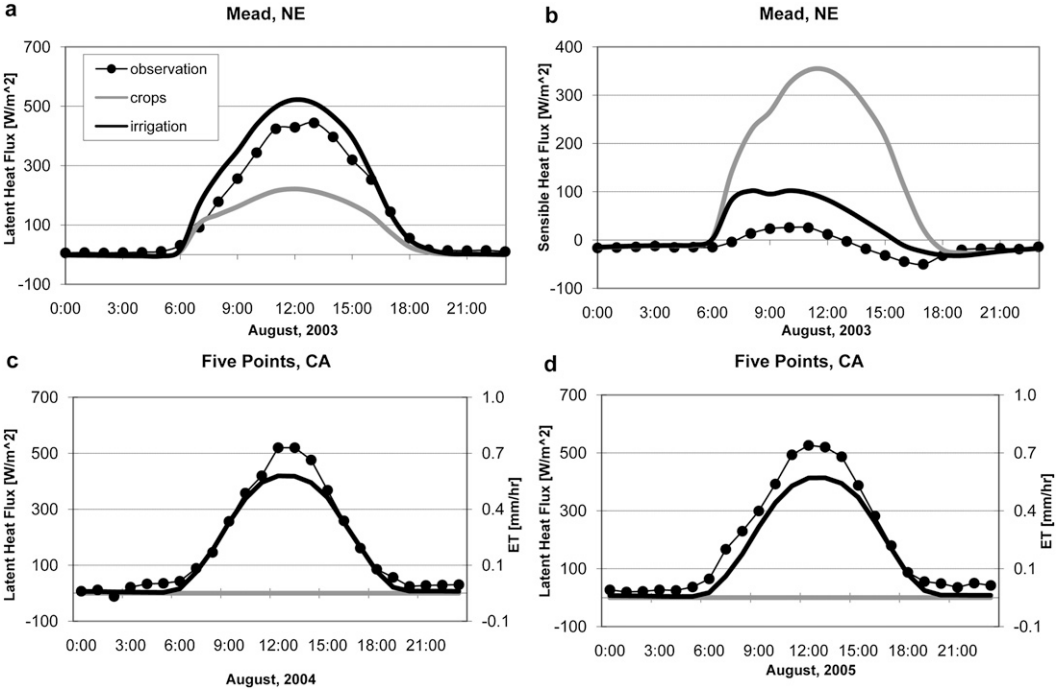

FIG. 7. Diurnal cycles of (a) latent–and (b) sensible–heat fluxes (W m^{-2}) at the Mead, Nebraska, AmeriFlux site averaged over August 2003, and (c) evapotranspiration (mm h^{-1}) averaged over August 2004 and (d) August 2005 at the USDA site near Five Points, California. Plotted are observations (dots) and output from the crops (gray line) and irrigation (black line) simulations.

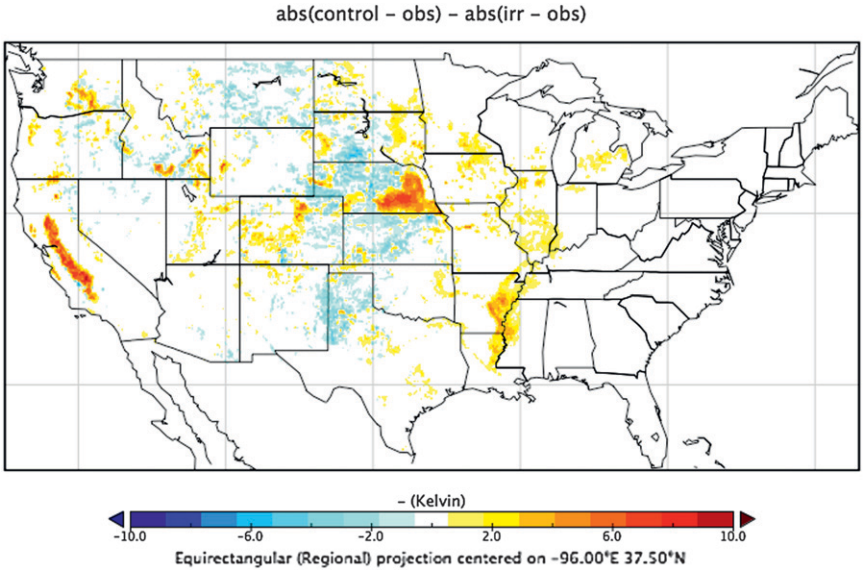

FIG. 8. Improvements in land surface temperature prediction errors represented as $\Delta LST_{model\text{-}obs} = |LST_{crops} - LST_{GOES}| - |LST_{irr} - LST_{GOES}|$. Both GOES data and predictions are averaged over the 13-day period between 13 and 25 Aug 2003 at 1800 UTC. Presence of positive (red) values indicates that the main improvement caused by irrigation is simulated land surface cooling to match observations over the same period. Note that there are differences in nonirrigated areas, but these areas are outside the scope of this paper.

highly variable (both in space and in time) land surface conditions, including soil moisture and temperature, which affect atmospheric stability and boundary layer growth. Many studies have shown that conditions at the land surface in certain regions govern the development of weather patterns and precipitation (e.g., Dirmeyer 2000; Koster et al. 2004). During the growing season in many agricultural regions, irrigation can completely transform the terrestrial water and energy budgets. Therefore, we expect that, through improved simulation of land surface conditions, the new irrigation scheme will lead to improved weather and climate forecasting skill when incorporated into NWP models, such as NOAA's GFS, especially when we implement a full water balance scheme that will account for irrigation sources. Furthermore, it can easily be adapted for use in other land surface and coupled modeling systems.

The results are also highly relevant to regional-to-global-scale water and energy cycle studies. Irrigated area accounts for 2.7% of the continental United States based on the MODIS-derived irrigation map. When averaged over the entire United States, the water and energy budget effects presented in section 5b are diluted accordingly. For example, the nationwide increase in QLE (ET) was 4%; that is still a significant change in the water and energy balances considering the scale. Further, because farmers irrigate more in dry months and years, if water is available, then irrigation may act to buffer otherwise variable land surface conditions and fluxes that would feed back to the evolution of weather patterns and other phenomena, such as droughts. Exploring this hypothesis will be an important direction for future work. To date, most continental-to-global-scale water and energy cycle studies have not attempted to quantify irrigation effects. Our results provide a way forward using a modeling approach that can simultaneously incorporate other large-scale observations as inputs and constraints, following the LDAS paradigm (Mitchell et al. 2004; Rodell et al. 2004).

Acknowledgments. This research was partially made possible by the U.S. National Research Council and NASA Postdoctoral Program (NPP) Fellowships awarded to Mutlu Ozdogan. Dr. Ozdogan also acknowledges generous computation and logistical support from the Hydrological Sciences Branch at NASA GSFC. GOES land surface temperature data were provided by Martha Anderson of ARS, USDA Maryland. The lysimeter data for California were provided by Dr. James Ayars of ARS, USDA California.

REFERENCES

Adegoke, J. O., R. A. Pielke, J. Eastman, R. Mahmood, and K. G. Hubbard, 2003: Impact of irrigation on midsummer surface fluxes and temperatures under dry synoptic conditions:

A regional atmospheric model study of the U.S. high plains. *Mon. Wea. Rev.,* **131,** 556–564.

Baldwin, M., and K. E. Mitchell, 1997: The NCEP hourly multisensor U.S. precipitation analysis for operations and GCIP research. Preprints, *13th Conf. on Hydrology,* Long Beach, CA, Amer. Meteor. Soc., 54–55.

Ben-Gai, T., A. Bitan, M. Manes, and P. Alpert, 2001: Climatic variations in the moisture and instability patterns of the atmospheric boundary layer on the East Mediterranean coastal plain of Israel. *Bound-Layer Meteor.,* **100,** 363–371.

Betts, A., F. Chen, K. Mitchell, and Z. Janjic, 1997: Assessment of the land surface and boundary layer models in two operational versions of the NCEP Eta model using FIFE data. *Mon. Wea. Rev.,* **125,** 2896–2916.

Bonan, G. B., 1997: Effects of Land Use on the Climate of the United States. *Climatic Change,* **37,** 449–486.

——, 2001: Observational evidence for reduction of daily maximum temperature by croplands in the Midwest United States. *J. Climate,* **14,** 2430–2442.

——, S. Levis, M. Sitch, M. Vertenstein, and K. W. Oleson, 2003: A dynamic global vegetation model for use with climate models: Concepts and description of simulated vegetation dynamics. *Global Change Biol.,* **9,** 1543–1566.

Chase, T. N., R. A. Pielke Sr., T. G. F. Kittel, R. Nemani, and S. W. Running, 2000: Simulated impacts of historical land cover changes on global climate in northern winter. *Climate Dyn.,* **16,** 93–105.

Chen, F., and R. Avissar, 1994: The impact of land-surface wetness heterogeneity on mesoscale heat fluxes. *J. Appl. Meteor.,* **33,** 1323–1340.

——, and Coauthors, 1996: Modeling of land surface evaporation by four schemes and comparison with FIFE observations. *J. Geophys. Res.,* **101** (D3), 7251–7268.

Cosgrove, B. A., and Coauthors, 2003: Real-time and retrospective forcing in the North American Land Data Assimilation System (NLDAS) project. *J. Geophys. Res.,* **108,** 8842, doi:10.1029/2002JD003118.

de Rosnay, P., J. Polcher, K. Laval, and M. Sabre, 2003: Integrated parameterization of irrigation in the land surface model ORCHIDEE. Validation over Indian Peninsula. *Geophys. Res. Lett.,* **30,** 1986, doi:10.1029/2003GL018024.

Dickinson, R. E., and A. Henderson-Sellers, 1988: Modelling tropical deforestation: A study of GCM land-surface parameterizations. *Quart. J. Roy. Meteor. Soc.,* **114,** 439–462.

Dirmeyer, P., 2000: Using a global soil wetness dataset to improve seasonal climate simulation. *J. Climate,* **13,** 2900–2922.

Ek, M. B., K. E. Mitchell, Y. Lin, E. Rogers, P. Grunmann, V. Koren, G. Gayno, and J. D. Tarpley, 2003: Implementation of Noah land surface model advances in the National Centers for Environmental Prediction operational mesoscale Eta model. *J. Geophys. Res.,* **108,** 8851, doi:10.1029/2002JD003296.

Gesch, D. B., K. L. Verdin, and S. K. Greenlee, 1999: New land surface digital elevation model covers the Earth. *Eos, Trans. Amer. Geophys. Union,* **80,** 69–70.

Haddeland, I., D. P. Lettenmaier, and T. Skaugen, 2006: Effects of irrigation on the water and energy balances of the Colorado and Mekong river basins. *J. Hydrol.,* **324,** 210–223.

Hansen, M. C., R. S. DeFries, J. R. G. Townshend, and R. Sohlberg, 2000: Global land cover classification at 1 km spatial resolution using a classification tree approach. *Int. J. Remote Sens.,* **21,** 1331.

Higgins, R. W., W. Shi, E. Yarosh, and R. Joyce, 2000: Improved United States precipitation quality control system and analysis. NCEP/Climate Prediction Center Atlas 7, Climate Prediction Center, Camp Springs, MD, 40 pp.

Hutson, S. S., N. L. Barber, J. F. Kenny, K. S. Linsey, D. S. Lumia, and M. A. Maupin, 2004: Estimated use of water in the United States in 2000. U.S. Geological Survey Circular 1268, USGS, 46 pp.

Kanamaru, H., and M. Kanamitsu, 2008: Model diagnosis of nighttime minimum temperature warming during summer due to irrigation in the California Central Valley. *J. Hydrometeor.,* **9,** 1061–1072.

Koren, V., J. Schaake, K. Mitchell, Q.-Y. Duan, F. Chen, and J. M. Baker, 1999: A parameterization of snowpack and frozen ground intended for NCEP weather and climate models. *J. Geophys. Res.,* **104,** 19 569–19 585.

Koster, R. D., and Coauthors, 2004: Regions of strong coupling between soil moisture and precipitation. *Science,* **305,** 1138–1140, doi:10.1126/science.1100217.

Kueppers, L. M., M. A. Snyder, and L. C. Sloan, 2007: Irrigation cooling effect: Regional climate forcing by land-use change. *Geophys. Res. Lett.,* **34,** L03703, doi:10.1029/2006GL028679.

——, and Coauthors, 2008: Seasonal temperature responses to land-use change in the western United States. *Global Planet. Change,* **60,** 250–264, doi:10.1016/j.gloplacha.2007.03.005.

Kumar, S. V., and Coauthors, 2006: Land information system: An interoperable framework for high resolution land surface modeling. *Environ. Model. Software,* **21,** 1402–1415.

Leff, B., N. Ramankutty, and J. A. Foley, 2004: Geographic distribution of major crops across the world. *Global Biogeochem. Cycles,* **18,** GB1009, doi:10.1029/2003GB002108.

Lobell, D. B., and C. Bonfils, 2008: The effect of irrigation on regional temperatures: A spatial and temporal analysis of trends in California, 1934–2002. *J. Climate,* **21,** 2063–2071.

——, G. Bala, and P. B. Duffy, 2006: Biogeophysical impacts of cropland management changes on climate. *Geophys. Res. Lett.,* **33,** L06708, doi:10.1029/2005GL025492.

——, C. Bonfils, and J. M. Faurès, 2008: The role of irrigation expansion in past and future temperature trends. *Earth Interactions,* **12.** [Available online at http://EarthInteractions.org.]

Mahmood, R., and K. G. Hubbard, 2002: Anthropogenic land-use change in the North American tall grass-short grass transition and modification of near-surface hydrologic cycle. *Climate Res.,* **21,** 83–90.

Mitchell, K., and Coauthors, 2004: The multi-institution North American Land Data Assimilation System (NLDAS): Utilizing multiple GCIP products and partners in a continental distributed hydrological modeling system. *J. Geophys. Res.,* **109,** D07S90, doi:10.1029/2003JD003823.

Moore, N., and S. Rojstaczer, 2002: Irrigation's influence on precipitation: Texas High Plains, U.S.A. *Geophys. Res. Lett.,* **29,** 1755, doi:10.1029/2002GL014940.

NOAA, cited 2005: ''Technical procedures bulletin'' for the T382 Global Forecast System. [Available online at http://www.emc.ncep.noaa.gov/gc_wmb/Documentation/TPBoct05/T382.TPB.FINAL.htm.]

Otterman, J., A. Manes, S. Rubin, P. Alpert, and D. O'C Starr, 1990: An increase of early rains in southern Israel following land-use change? *Bound.-Layer Meteor.,* **53,** 333–351.

Ozdogan, M., and G. Gutman, 2008: A new methodology to map irrigated areas using multi-temporal MODIS and ancillary data: An application example in the continental US. *Remote Sens. Environ.,* **112,** 3520–3537.

——, G. D. Salvucci, and B. C. Anderson, 2006: Examination of the Bouchet–Morton complementary relationship using a mesoscale climate model and observations under a progressive irrigation scenario. *J. Hydrometeor.,* **7,** 235–251.

Pielke, R. A., and X. Zeng, 1989: Influence of severe storm development of irrigated land. *Natl. Wea. Dig.,* **14,** 16–17.

Pinker, R. T., and Coauthors, 2003: Surface radiation budgets in support of the GEWEX Continental-Scale International Project (GCIP) and the GEWEX Americas Prediction Project (GAPP), including the North American Land Data Assimilation System (NLDAS) project. *J. Geophys. Res.,* **108,** 8844, doi:10.1029/2002JD003301.

Reynolds, C. A., T. J. Jackson, and W. J. Rawls, 2000: Estimating soil water-holding capacities by linking the Food and Agriculture Organization Soil Map of the World with global pedon databases and continuous pedotransfer functions. *Water Resour. Res.,* **36,** 3653–3662.

Rodell, M., and Coauthors, 2004: The Global Land Data Assimilation System. *Bull. Amer. Meteor. Soc.,* **85,** 381–394.

Rogers, E., T. L. Black, D. G. Deaven, G. J. DiMego, Q. Zhao, M. Baldwin, N. W. Junker, and Y. Lin, 1996: Changes to the operational ''early'' eta analysis/forecast system at the National Centers for Environmental Prediction. *Wea. Forecasting,* **11,** 391–413.

Segal, M., Z. Pan, R. W. Turner, and E. S. Takle, 1998: On the potential impact of irrigated areas in North American summer rainfall caused by large-scale systems. *J. Appl. Meteor.,* **37,** 325–331.

Sellers, P. J., and Coauthors, 1996: A revised land surface parameterization (SiB2) for atmospheric GCMs. Part I: Model formulation. *J. Climate,* **9,** 676–705.

Siebert, S., P. Döll, S. Feick, J. Hoogeveen, and K. Frenken, 2007: Global map of irrigated areas version 4.0.1. University of Frankfurt (Main), Germany/Food and Agriculture Organization of the United Nations, Rome, Italy. [Available online at http://www.fao.org/nr/water/aquastat/irrigationmap/index10.stm.]

Tang, Q., T. Oki, S. Kanae, and H. Hu, 2007: The influence of precipitation variability and partial irrigation within grid cells on a hydrological simulation. *J. Hydrometeor.,* **8,** 499–512.

Thenkabail, P. S., and Coauthors, 2008: A global irrigated area map (GIAM) using remote sensing at the end of the last millennium. International Water Management Institute Rep., 63 pp.

USDA, 2004: Census of agriculture 2002: Farm and ranch irrigation survey (2003), Vol. 3, Special Studies, Part 1, USDA Tech. Rep., NTIS AC-02-SS-1, 216 pp.

Vaughan, P. J., T. J. Trout, and J. E. Ayars, 2007: A processing method for weighing lysimeter data and comparison to micrometeorological ETo predictions. *Agric. Water Manage.,* **88,** 141–146.

Weare, B. C., and H. Du, 2008: Modelling regional climate changes: Influences of recent global warming and irrigation in California. *Int. J. Climatol.,* **28,** 1201–1212.

Yeh, T. C., R. T. Wetherald, and S. Manabe, 1984: Effect of soil moisture on the short-term climate and hydrology change: A numerical experiment. *Mon. Wea. Rev.,* **112,** 474–490.